

# Noncommutative geometry and the primordial dipolar imaginary power spectrum

Pankaj Jain<sup>a</sup>, Pranati K. Rath<sup>b</sup>

Department of Physics, Indian Institute of Technology Kanpur, Kanpur 208016, India

Received: 8 July 2014 / Accepted: 26 February 2015 / Published online: 11 March 2015  
© The Author(s) 2015. This article is published with open access at Springerlink.com

**Abstract** We argue that noncommutative space-times lead to an anisotropic dipolar imaginary primordial power spectrum. We define a new product rule, which allows us to consistently extract the power spectrum in such space-times. The precise nature of the power spectrum depends on the model of noncommutative geometry. We assume a simple dipolar model which has a power dependence on the wave number,  $k$ , with a spectral index,  $\alpha$ . We show that such a spectrum provides a good description of the observed dipole modulation in the cosmic microwave background radiation (CMBR) data with  $\alpha \approx 0$ . We extract the parameters of this model from the data. The dipole modulation is related to the observed hemispherical anisotropy in the CMBR data, which might represent the first signature of quantum gravity.

## 1 Introduction

The cosmic microwave background radiation (CMBR) shows a hemispherical power anisotropy [1–9], which can be parameterized as,

$$\Delta T(\hat{n}) = g(\hat{n})(1 + A\hat{\lambda} \cdot \hat{n}) \quad (1)$$

where  $g(\hat{n})$  is an isotropic and Gaussian random field,  $\hat{\lambda}$  the preferred direction and  $A$  the amplitude of anisotropy. This model implies a dipole modulation [10–13] of the CMBR temperature field. The WMAP 5 year data leads to  $A = 0.072 \pm 0.022$  with the dipole direction,  $(l, b) = (224^\circ, -22^\circ) \pm 24^\circ$  for  $l \leq 64$  in the galactic coordinates [1–4, 6, 8]. This anisotropy has been confirmed by PLANCK [7] with amplitude,  $A = 0.073 \pm 0.010$ , and direction  $(l, b) = (217^\circ, -20^\circ) \pm 15^\circ$  for  $l \leq 64$ . It has been shown in [14] that the model, Eq. (1), leads to several additional implications for CMBR, besides hemispherical anisotropy.

The hemispherical anisotropy has also been probed at multipoles higher than 64 [4, 5]. The signal is found to be absent at  $l \sim 500$  [15, 16] and also not seen in the large scale structures [17, 18]. These observations may be accommodated in a model which proposes a scale dependent power spectrum [19], such that the effect is negligible at high  $l$ .

Many theoretical models, such as, [20–44], have been proposed which aim to explain the observed hemispherical anisotropy as well as other signals of anisotropy seen in data [45–51]. An interesting possibility is that there might have been a phase of anisotropic expansion at very early time. The inflationary Big Bang cosmology is perfectly consistent with such an evolution [52]. The anisotropic modes, generated during this early phase may later re-enter the horizon [52, 53] and lead to the observed signals.

In this paper our objective is to determine a primordial power spectrum which may lead to dipole modulation and hence hemispherical anisotropy. It is possible to find a power spectrum based on an inhomogeneous model [3, 17, 32, 54–56] which is consistent [57] with the observed temperature anisotropy. However, it is not clear how an anisotropic model might lead to a dipole modulation. The simplest model that one might construct leads to quadrupolar and not dipolar modulation [57]. The basic problem can be understood by considering the two point correlations in real space. Let  $\delta(\vec{x})$  be the density fluctuations in real space. Their two point correlation function,  $F(\vec{\Delta}, \vec{X})$ , may be expressed as

$$F(\vec{\Delta}, \vec{X}) = \langle \delta(\vec{x})\delta(\vec{x}') \rangle \quad (2)$$

where  $\vec{\Delta} = \vec{x} - \vec{x}'$  and  $\vec{X} = (\vec{x} + \vec{x}')/2$ . We are interested in a correlation which is anisotropic and hence depends on  $\vec{\Delta}$  besides the magnitude  $\Delta \equiv |\vec{\Delta}|$ . It is clear from the definition of the correlation function that, in a classical framework, it must satisfy

$$\langle \delta(\vec{x})\delta(\vec{x}') \rangle = \langle \delta(\vec{x}')\delta(\vec{x}) \rangle \quad (3)$$

Hence it can only be an even function of  $\vec{\Delta}$ . The simplest anisotropic function is, therefore,

<sup>a</sup> e-mail: [pkjain@iitk.ac.in](mailto:pkjain@iitk.ac.in)

<sup>b</sup> e-mail: [pranati@iitk.ac.in](mailto:pranati@iitk.ac.in)

$$F(\vec{\Delta}, \vec{X}) = f_1(\Delta) + B_{ij} \Delta_i \Delta_j f_2(\Delta) \tag{4}$$

where  $B_{i,j}, i, j = 1, 2, 3$  are parameters. It is clear that such a model cannot give rise to a dipole modulation, which requires a term linear in  $\Delta_i$ .

In this paper we argue that in a noncommutative space-time, a term linear in  $\Delta_i$  is permissible. The power spectrum that we are interested in is applicable at very early time, perhaps even the time when quantum gravity effects were not negligible. At that time, we cannot assume that space-time is commutative [58–62]. Its noncommutativity may be expressed as

$$[\hat{x}_\mu, \hat{x}_\nu] = i\theta_{\mu\nu} \tag{5}$$

where  $\theta_{\mu\nu}$  are parameters and the coordinate functions,  $\hat{x}_\mu(x)$ , depend on the choice of coordinate system. In a particular coordinate system, we may set

$$\hat{x}_\mu(x) = x_\mu. \tag{6}$$

In [63] the authors assume that this preferred system is the comoving coordinate system. In general, the noncommutativity can appear quite complicated in different systems. The effect of noncommutativity on cosmology has been considered earlier [63–79]. However, as explained below, the results obtained in our paper are new.

In [57], we have determined the power spectrum corresponding to an inhomogeneous model and shown that its spectral index is consistent with zero. In the present paper we determine the power spectrum of an anisotropic model based on noncommutative space-time.

### 2 Correlations induced by dipole modulation

In this section we review the correlations between different multipoles which are induced by the dipole modulation model, Eq. (1). We may expand the CMBR temperature as

$$\Delta T(\hat{n}) = \sum_{lm} a_{lm} Y_{lm}(\hat{n}) \tag{7}$$

where  $a_{lm}$  are the spherical harmonic coefficients. Their two point correlation function may be expressed as [14],

$$\langle a_{lm} a_{l'm'}^* \rangle = \langle a_{lm} a_{l'm'}^* \rangle_{\text{iso}} + \langle a_{lm} a_{l'm'}^* \rangle_{\text{dm}} \tag{8}$$

where

$$\begin{aligned} \langle a_{lm} a_{l'm'}^* \rangle_{\text{iso}} &= C_l \delta_{ll'} \delta_{mm'} \\ \langle a_{lm} a_{l'm'}^* \rangle_{\text{dm}} &= A (C_{l'} + C_l) \xi_{lm;l'm'}^0 \end{aligned} \tag{9}$$

Here  $C_l$  is the standard angular power spectrum,  $\langle a_{lm} a_{l'm'}^* \rangle_{\text{dm}}$  is the contribution due to the anisotropic dipole modulation and

$$\begin{aligned} \xi_{lm;l'm'}^0 &= \delta_{m',m} \left[ \sqrt{\frac{(l-m+1)(l+m+1)}{(2l+1)(2l+3)}} \delta_{l',l+1} \right. \\ &\quad \left. + \sqrt{\frac{(l-m)(l+m)}{(2l+1)(2l-1)}} \delta_{l',l-1} \right]. \end{aligned} \tag{10}$$

Hence the model leads to correlations between multipoles,  $l$  and  $l + 1$ . We define the statistic [14],

$$S_H(L) = \sum_{l=l_{\min}}^L \frac{l(l+1)}{2l+1} \sum_{m=-l}^l a_{lm} a_{l+1,m}^*. \tag{11}$$

We maximize the statistic by varying over the direction parameters. The resulting statistic is labeled as  $S_H^{\text{data}}$ . This provides a measure of the signature of anisotropy seen in the data. This can be compared with a theoretical power spectrum model in order to fix its parameters.

### 3 Anisotropic power spectrum

The relationship between the temperature fluctuations,  $\Delta T(\hat{n})$ , and the primordial density perturbations,  $\delta(\vec{k})$ , can be expressed as

$$\frac{\Delta T}{T_0}(\hat{n}) = \int d^3k \sum_l (-i)^l (2l+1) \delta(k) \Theta_l(k) P_l(\hat{k} \cdot \hat{n}) \tag{12}$$

where  $P_l(\hat{k} \cdot \hat{n})$  are the Legendre polynomials,

$$P_l(\hat{n} \cdot \hat{n}') = \frac{4\pi}{2l+1} \sum_m Y_{lm}(\hat{n}) Y_{lm}^*(\hat{n}'), \tag{13}$$

$\Theta_l(k)$  the transfer function and  $k = |\vec{k}|$ . Here we assume an approximate form of the transfer function,  $\Theta_l(k) = \frac{3}{10} j_l(k\eta_0)$  [80], where  $j_l$  is the spherical Bessel function and  $\eta_0$  is the current conformal time. This form of the transfer function is obtained by including only the contribution from the Sachs–Wolfe effect. In this paper we confine ourselves to the low- $l$  multipoles,  $l \leq 64$ , for which this is sufficiently reliable. The error induced by ignoring other contributions is smaller than the error in our extracted parameters, which, as we shall see, is of the order of 25 %. It is of course necessary to improve the accuracy of our calculation, as well as to extend it to higher multipoles. This computation is complicated and we prefer to postpone it for future research. There also appears to be some evidence that the signal decays for larger values of  $l$  [76]. This provides additional motivation for confining our computation for  $l \leq 64$ .

We next propose the following form of the anisotropic power spectrum in real space:

$$F(\vec{\Delta}) = f_1(\Delta) + \hat{\lambda} \cdot \vec{\Delta} f_2(\Delta) \tag{14}$$

where  $\hat{\lambda}$  represents the preferred direction and  $f_1$  and  $f_2$  depend only on the magnitude  $\Delta$ . Such a form is gener-

ally not permissible since the correlation function must satisfy Eq. (3). However, this does not follow in noncommutative space-time [63]. In this case the relevant quantity is the deformed quantum field. Let  $\varphi_0(\vec{x}, t)$  be a self-adjoint scalar field. The deformed quantum field is defined as [63]

$$\varphi_\theta = \varphi_0 e^{\frac{1}{2} \overleftarrow{\partial} \wedge P} \tag{15}$$

where

$$\overleftarrow{\partial} \wedge P \equiv \overleftarrow{\partial}_\mu \theta^{\mu\nu} P_\nu \tag{16}$$

and  $P_\mu$  is the Fock space momentum operator [63]. In these equations the arrow pointing left means that the derivative acts on the fields appearing on the left of this operator. For a deformed field,

$$\varphi_\theta(\mathbf{x}, t)\varphi_\theta(\mathbf{x}', t') \neq \varphi_\theta(\mathbf{x}', t')\varphi_\theta(\mathbf{x}, t) \tag{17}$$

even for space-like separations [63]. Hence Eq. (3) does not follow and a correlation function, Eq. (14), which depends linearly on  $\vec{\Delta}$ , is permissible.

The correlation function of the Fourier transform,  $\delta(\vec{k})$ , of  $\vec{\delta}(\vec{x})$  may be expressed as

$$\langle \delta(\vec{k})\delta^*(\vec{k}') \rangle = \int \frac{d^3 X}{(2\pi)^3} \frac{d^3 \Delta}{(2\pi)^3} e^{i(\vec{k}+\vec{k}')\cdot\vec{\Delta}/2} e^{i(\vec{k}-\vec{k}')\cdot\vec{X}} \times F(\vec{\Delta}, \vec{X}). \tag{18}$$

Using the model given in Eq. (14), we obtain

$$\langle \delta(\vec{k})\delta^*(\vec{k}') \rangle = \delta^3(\vec{k} - \vec{k}') \int d^3 \Delta e^{i(\vec{k}+\vec{k}')\cdot\vec{\Delta}/2} F(\vec{\Delta}). \tag{19}$$

This leads to

$$\langle \delta(\vec{k})\delta^*(\vec{k}') \rangle = \delta^3(\vec{k} - \vec{k}') P(k) [1 + i(\hat{k} \cdot \hat{\lambda})g(k)] \tag{20}$$

where the delta function arises due to spatial translational invariance and  $P(k)$  is the Fourier transform of  $f_1(\Delta)$ . The anisotropic component of the power spectrum,  $g(k)$ , can be expressed as

$$g(k) = -\frac{1}{P(k)} \frac{df_2(k)}{dk} \tag{21}$$

where  $\tilde{f}_2(k)$  is the Fourier transform of  $f_2(\Delta)$ . Here  $P(k)$  is the standard power spectrum,

$$P(k) = k^{n-4} A_\phi / (4\pi). \tag{22}$$

Here we set the parameters  $n = 1$  and  $A_\phi = 1.16 \times 10^{-9}$  [80]. In Eq. (21),  $g(k)$  is a real function which depends only on the magnitude  $k = |\vec{k}|$  and represents the violation of statistical isotropy. A more detailed fit, with  $n$  different from unity, is postponed to future work.

### 3.1 A model power spectrum in noncommutative space-time

We have so far argued that a noncommutative space-time leads to an imaginary component in the power spectrum. In the present section we use the model proposed in [63] in order to compute the corresponding power spectrum. As explained in Sect. 1, this model assumes that the coordinates appearing in the basic equation, Eq. (5), are the comoving coordinates in the FRW metric. Following the notation of [63], we denote the inflaton field by  $\varphi(\vec{x}, t)$ . We expand it around the background field,  $\varphi^0(t)$ , so that

$$\varphi(\vec{x}, t) = \varphi^{(0)}(t) + \delta\varphi(\vec{x}, t). \tag{23}$$

We denote the Fourier transform of  $\delta\varphi(\vec{x}, t)$  by  $\Phi(\vec{k}, t)$ , i.e.,

$$\Phi(\vec{k}, t) = \int d^3x \delta\varphi(\vec{x}, t) e^{-i\vec{k}\cdot\vec{x}}. \tag{24}$$

It is useful to define the field  $\tilde{\Phi}(\vec{k}, \eta) = a(\eta)\Phi(\vec{k}, \eta)$ , where  $a(\eta)$  is the cosmic scale factor and  $\eta = \eta(t)$  is the conformal time. We can express this field in terms of the creation and annihilation operators as

$$\tilde{\Phi}(\vec{k}, \eta) = u(\vec{k}, \eta)\hat{a}(\vec{k}) + u^*(-\vec{k}, \eta)a^\dagger(-\vec{k}) \tag{25}$$

where  $u(\vec{k}, \eta)$  is the standard mode function,

$$u(\vec{k}, \eta) = \frac{e^{-ik\eta}}{\sqrt{2k}} \left( 1 - \frac{i}{k\eta} \right). \tag{26}$$

We need to include only the second term in the brackets in this equation since it dominates at horizon crossing.

The resulting power spectrum is given in [74] for the commutator,

$$\frac{1}{2} [\Phi_\theta(\vec{k}, \eta), \Phi_\theta(\vec{k}', \eta)]_- \equiv \frac{1}{2} (\Phi_\theta(\vec{k}, \eta)\Phi_\theta(\vec{k}', \eta) - \Phi_\theta(\vec{k}', \eta)\Phi_\theta(\vec{k}, \eta)) \tag{27}$$

where  $\eta$  is the conformal time and  $\Phi_\theta$  represent the deformed quantum field, as defined in Eq. (15). In Fourier space the power spectrum is given by Eq. (17) of [74], reproduced here for convenience,

$$\frac{1}{2} \langle 0 | [\Phi_\theta(\vec{k}, \eta), \Phi_\theta(\vec{k}', \eta)]_- | 0 \rangle \Big|_{\text{horizon crossing}} = (2\pi)^3 P(k) \sinh(H\vec{\theta}^0 \cdot \vec{k}) \delta(\vec{k} + \vec{k}'). \tag{28}$$

Surprisingly, this power spectrum is real. Such a power spectrum would produce unphysical results and cannot arise in a sensible theory. It clearly represents some error in the calculation. Before correcting this crucial error in this equation we explain the different terms. The function  $P(k)$  is the standard

power spectrum, given in Eq. (22) and  $\vec{\theta}^0 = (\theta^{01}, \theta^{02}, \theta^{03})$  are three parameters. The argument of the Dirac delta function is  $(\vec{k} + \vec{k}')$  instead of  $(\vec{k} - \vec{k}')$  in Eq. (19), since here we take the correlation between  $\Phi_\theta(\vec{k}, \eta)$  and  $\Phi_\theta(\vec{k}', \eta)$  instead of  $\Phi_\theta(\vec{k}, \eta)$  and  $\Phi_\theta^\dagger(\vec{k}', \eta)$ .

The fact that the power spectrum odd in  $\vec{k}$  must be imaginary has already been recognized in [75]. In this paper one cures this problem by a prescription, Eq. (3.13) of [75], where the correlation is simply defined to have an imaginary component. To be precise the correlator of the anti-self-adjoint part of the operator is multiplied by the imaginary  $i$ . This is an interesting suggestion. It correctly points out the basic problem that the operator whose expectation value is being computed is not Hermitian. However, it is not clear how this suggestion can be implemented at a fundamental level. The action of any operator on a state is well defined. Hence it is not clear how one can have different definitions of expectation values for different parts of an operator. It is clear that the problem is not really solved and we need to look for alternatives. In the second model discussed in [75], again the parity odd power spectrum, Eq. (4.11) of [75], turns out to be real. It acquires an imaginary component only if the vector  $\vec{v} = H\vec{\theta}$  is chosen to be imaginary, as explained in the discussion following Eq. (4.11) of that paper. Here  $H$  is the Hubble parameter and  $\vec{\theta}$  is the same as the vector  $\vec{\theta}^0$ , defined in the previous paragraph. However, our main point is that we need to obtain an imaginary power spectrum with  $\vec{\theta}^0$  a real vector. Here  $H$  is of course necessarily real.

As we have discussed above, the basic problem is traced to the fact that the quantity being computed is not Hermitian and hence not an observable. We next demonstrate this explicitly. Let  $\phi_0(\vec{x}, t)$  represent a real scalar quantum field and  $\phi_\theta(\vec{x}, t)$  the corresponding  $\theta$  deformed field. The quantity which was computed in [63], in position space, is the vacuum expectation value of the product of two fields, i.e.,

$$\langle 0 | \phi_\theta(\vec{x}_1, t_1) \phi_\theta(\vec{x}_2, t_2) | 0 \rangle \tag{29}$$

where the deformed product is explicitly given in Eq. (3.14) of [63]. For the product of two fields, it is given by

$$\begin{aligned} &\langle 0 | \phi_\theta(\vec{x}_1, t_1) \phi_\theta(\vec{x}_2, t_2) | 0 \rangle \\ &= \langle 0 | \phi_0(\vec{x}_1, t_1) \phi_0(\vec{x}_2, t_2) | 0 \rangle e^{-\frac{i}{2} \overleftarrow{\partial}_{x_2} \wedge \overleftarrow{\partial}_{x_1}}. \end{aligned} \tag{30}$$

This expectation value is proportional to the power in position space. This power should be compared with the basic equation, Eq. (14), and must be real in order to produce physically acceptable results. However, the problem is that this expectation value is not real since the operator under consideration is not Hermitian. This can easily be seen. We have

$$\begin{aligned} \phi_\theta(x_1) \phi_\theta(x_2) &= \phi_0(x_1) \phi_0(x_2) - \frac{i}{2} \frac{\partial}{\partial x_2^\mu} \phi_0(x_2) \theta^{\mu\nu} \\ &\times \frac{\partial}{\partial x_1^\nu} \phi_0(x_1) + \dots \end{aligned} \tag{31}$$

where we have kept terms only to leading order in  $\theta^{\mu\nu}$ . Here the arguments,  $x_1$  and  $x_2$ , denote both the space and the time coordinates, i.e.  $\phi_0(x_1) = \phi_0(\vec{x}_1, t_1)$  and  $\phi_0(x_2) = \phi_0(\vec{x}_2, t_2)$ , etc. Hence we find

$$\begin{aligned} (\phi_\theta(x_1) \phi_\theta(x_2))^\dagger &= \phi_0(x_2) \phi_0(x_1) + \frac{i}{2} \frac{\partial}{\partial x_1^\nu} \phi_0(x_1) \theta^{\mu\nu} \\ &\times \frac{\partial}{\partial x_2^\mu} \phi_0(x_2) + \dots \end{aligned} \tag{32}$$

where we have used the fact that  $\phi_0(x)^\dagger = \phi_0(x)$ . Since  $\phi_0(\vec{x}_1, t_1)$  and  $\phi_0(\vec{x}_2, t_2)$  commute for space-like separations, we obtain

$$\begin{aligned} (\phi_\theta(x_1) \phi_\theta(x_2))^\dagger &= \phi_0(x_1) \phi_0(x_2) + \frac{i}{2} \frac{\partial}{\partial x_2^\mu} \phi_0(x_2) \theta^{\mu\nu} \\ &\times \frac{\partial}{\partial x_1^\nu} \phi_0(x_1) + \dots \neq \phi_\theta(x_1) \phi_\theta(x_2). \end{aligned} \tag{33}$$

Hence we see that  $\phi_\theta(\vec{x}_1, t_1) \phi_\theta(\vec{x}_2, t_2)$  is not a Hermitian operator and its vacuum expectation value is not physically observable. The same applies to the vacuum expectation value of this operator in Fourier space. In view of this it is not surprising that it does not lead to sensible results.

In order to cure this problem we define a new twist element, given by

$$\mathcal{F}_{\theta_R} = \exp\left(-\frac{1}{2} \theta^{\alpha\beta} P_\alpha \otimes P_\beta\right) \tag{34}$$

with  $P_\alpha = -i \partial_\alpha$ . In contrast to Eq. (2.4) of [63], this does not carry an  $i$  in the exponent. We call this the real twist element. This twist element leads us to define a new product of two functions,  $f(x)$  and  $g(x)$ . Here the argument  $x$  denotes both the space and the time coordinates, i.e.  $(\vec{x}, t)$ . We define

$$(f \diamond g)(x) = [e^{-\frac{1}{2} \theta^{\mu\nu} P_\mu \otimes P_\nu} f \otimes g](x), \tag{35}$$

which we call the diamond product, in contrast to the star product, defined in Eq. (2.10) of [63]. The product symbol,  $\otimes$ , has the same meaning as in [63]. This implies that the right hand side has to be evaluated by acting with the first operator  $P_\mu (= -i \partial_\mu)$  on the function  $f(x)$  and the second operator  $P_\nu (= -i \partial_\nu)$  on  $g(x)$ . We point out that this is simply an additional product rule, besides the standard star product, that we can define within the framework of noncommutative space-time. It does not conflict with any rule of noncommutative geometry or quantum mechanics. For example, one can always take a scalar or vector product of ordinary vectors, without being in conflict with any of the rules of vector algebra.

We emphasize that it is not necessary that only the star product must be taken while computing the power. The use of a star product in [63] was only a prescription. The fundamental theory in noncommutative space-time is defined by

converting all products in the action into star products. However, this does not imply that only those operators can be constructed which involve star products. The precise operator that should arise while computing the power spectrum must be consistently prescribed by the underlying field theory. One may, for example, use perturbation theory [21, 53] and compute the corrections to the power spectrum arising due to noncommutative space-time order by order in the noncommutative parameter,  $\bar{\theta}^0$ . This is rather complicated and we postpone this detailed calculation to future research. Here our use of the diamond product is a phenomenological prescription which is consistent with all rules of quantum field theory and noncommutative geometry. We expect that this would lead to correct results at least to leading order in the parameter  $\bar{\theta}^0$ .

Let us denote the deformed quantum field under the real twist element by  $\phi_{\theta_R}(\vec{x}, t)$ . Following [63], we can express the product of deformed fields in terms of the undeformed fields,  $\phi_0(\vec{x}, t)$ . We obtain

$$\phi_{\theta_R}(\vec{x}_1, t_1)\phi_{\theta_R}(\vec{x}_2, t_2) = \phi_0(\vec{x}_1, t_1)\phi_0(\vec{x}_2, t_2)e^{-\frac{i}{2}\overleftarrow{\partial}_{x_2}\wedge\overleftarrow{\partial}_{x_1}}. \tag{36}$$

The expectation value of this product in position space is real and hence provides a consistent generalization of the power in noncommutative spaces. We next explicitly show that the resulting power is real in position space. For this we only need to show that the real deformed product of two fields, Eq. (36), is Hermitian. We have

$$\begin{aligned} \phi_{\theta_R}(x_1)\phi_{\theta_R}(x_2) &= \phi_0(x_1)\phi_0(x_2) \\ &\quad - \frac{1}{2}\frac{\partial}{\partial x_2^\mu}\phi_0(x_2)\theta^{\mu\nu}\frac{\partial}{\partial x_1^\nu}\phi_0(x_1) + \dots \end{aligned} \tag{37}$$

where, for simplicity, we keep terms only to first order in  $\theta^{\mu\nu}$ . We have

$$\begin{aligned} (\phi_{\theta_R}(x_1)\phi_{\theta_R}(x_2))^\dagger &= \phi_0(x_2)\phi_0(x_1) \\ &\quad - \frac{1}{2}\frac{\partial}{\partial x_1^\nu}\phi_0(x_1)\theta^{\mu\nu}\frac{\partial}{\partial x_2^\mu}\phi_0(x_2) + \dots \\ &= \phi_0(x_1)\phi_0(x_2) \\ &\quad - \frac{1}{2}\frac{\partial}{\partial x_2^\mu}\phi_0(x_2)\theta^{\mu\nu}\frac{\partial}{\partial x_1^\nu}\phi_0(x_1) + \dots \\ &= \phi_{\theta_R}(x_1)\phi_{\theta_R}(x_2) \end{aligned} \tag{38}$$

where we have used  $\phi_0(x)^\dagger = \phi_0(x)$  and the fact that  $\phi_0(\vec{x}_1, t_1)$  and  $\phi_0(\vec{x}_2, t_2)$  commute for space-like separations. Here we have confined our proof to leading order in  $\theta^{\mu\nu}$ . It is clear that the proof will work to all orders. We simply need to expand the exponential to higher orders. At each order the operator is Hermitian, since the fields commute for space-like separations. However, we postpone a detailed discussion of

higher orders to a future publication. Furthermore we emphasize that our phenomenological prescription may be reliable only to leading order in  $\bar{\theta}^0$ .

We next return to the calculation of the power spectrum for the expanding Universe. This is now straightforward. We can directly extract the result from [63] by changing  $\bar{\theta}^0$  to  $i\bar{\theta}^0$ . In Fourier space we obtain

$$\begin{aligned} &\langle 0|\Phi_{\theta_R}(\vec{k}_1, t_1)\Phi_{\theta_R}(\vec{k}_2, t_2)|0\rangle \\ &= \left\langle 0\left|\Phi_0\left(\vec{k}_1, t_1 - i\frac{\bar{\theta}^0 \cdot \vec{k}_1}{2}\right)\Phi_0\left(\vec{k}_2, t_2 - i\frac{\bar{\theta}^0 \cdot \vec{k}_1}{2}\right)\right|0\right\rangle. \end{aligned} \tag{39}$$

This may be computed by first computing the expectation value for  $\bar{\theta}^0 = 0$  and then replacing  $t_1$  and  $t_2$  by  $t_1 - i\frac{\bar{\theta}^0 \cdot \vec{k}_1}{2}$  and  $t_2 - i\frac{\bar{\theta}^0 \cdot \vec{k}_1}{2}$ , respectively. This leads to

$$\begin{aligned} &\langle 0|\Phi_{\theta_R}(\vec{k}, \eta)\Phi_{\theta_R}(\vec{k}', \eta)|0\rangle \\ &= (2\pi)^3 P(k)e^{-iH\bar{\theta}^0 \cdot \vec{k}}\delta(\vec{k} + \vec{k}') \end{aligned} \tag{40}$$

$$\approx (2\pi)^3 P(k)(1 - iH\bar{\theta}^0 \cdot \vec{k})\delta(\vec{k} + \vec{k}') \tag{41}$$

at horizon crossing. In arriving at this result we have followed [63] and used the equations

$$\eta^\pm(\vec{k}) = \eta\left(t \pm \frac{i\bar{\theta}^0 \cdot \vec{k}}{2}\right) = \eta(t)e^{\mp\frac{i}{2}H\bar{\theta}^0 \cdot \vec{k}}. \tag{42}$$

We point out that in computing the power spectrum, it is useful to first express the two fields in terms of  $t_1$  and  $t_2$  as in Eq. (39) and then translate the time variables as indicated in this equation. The approximate equality, Eq. (41), where we retain only the term linear in  $\theta^{\mu\nu}$ , is valid for small  $k$ . Hence for small  $k$  we find an anisotropic power spectrum proportional to  $1/k^2$ . The leading order term leads to the standard power spectrum corresponding to an isotropic and homogeneous model.

The main point of the above calculation is that we can consistently obtain the imaginary dipolar power spectrum which is required to yield physically acceptable results. By comparing with Eq. (20), we identify

$$\begin{aligned} \hat{\lambda} &= -\frac{\bar{\theta}^0}{|\bar{\theta}^0|} \\ g(k) &= kH|\bar{\theta}^0| \end{aligned} \tag{43}$$

in the limit of small  $k$ . Hence we find that in this limit the anisotropic term increases linearly with  $k$ .

The precise form of the correlation predicted within the framework of noncommutative geometry is model dependent. In particular, the basic equation, Eq. (5), depends on the choice of coordinates which obey this simple relationship. Here we do not confine ourselves to a particular model and instead extract the anisotropic power directly from the

data. For this purpose, we assume the following parametrization of  $g(k)$ :

$$g(k) = g_0(k\eta_0)^{-\alpha} \tag{44}$$

where  $g_0$  and  $\alpha$  are parameters. The noncommutative model, Eq. (5), implies  $\alpha = -1$ . As we shall see the data indicates a value of  $\alpha$  close to zero for the range of  $l$  explored in this paper.

### 3.2 Implications for CMB temperature anisotropy

We next compute the two point temperature correlations,

$$\begin{aligned} \langle \Delta T(\hat{n}) \Delta T(\hat{n}') \rangle &= T_0^2 \int d^3k \sum_{l,l'=0}^{\infty} (-i)^{l-l'} \\ &\times (2l+1)(2l'+1) \Theta_l(k) \Theta_{l'}(k) \\ &\times P_l(\hat{k} \cdot \hat{n}) P_{l'}(\hat{k} \cdot \hat{n}') P_{\text{iso}}(k) [1 + i(\hat{k} \cdot \hat{\lambda}) g(k)]. \end{aligned} \tag{45}$$

Setting  $z$ -axis as the preferred direction, we obtain  $\hat{k} \cdot \hat{\lambda} = \cos \theta$ . The correlations of the spherical harmonic coefficients can be expressed as

$$\langle a_{lm} a_{l'm'}^* \rangle = \int d\Omega_{\hat{n}} d\Omega_{\hat{n}'} Y_{lm}^*(\hat{n}) Y_{l'm'}(\hat{n}') \langle \Delta T(\hat{n}) \Delta T(\hat{n}') \rangle. \tag{46}$$

We obtain

$$\langle a_{lm} a_{l'm'}^* \rangle = \langle a_{lm} a_{l'm'}^* \rangle_{\text{iso}} + \langle a_{lm} a_{l'm'}^* \rangle_{\text{aniso}}, \tag{47}$$

where

$$\langle a_{lm} a_{l'm'}^* \rangle_{\text{iso}} = (4\pi)^2 \frac{9T_0^2}{100} \delta_{ll'} \delta_{mm'} \int_0^{\infty} k^2 dk j_l^2(k\eta_0) P_{\text{iso}}(k), \tag{48}$$

$$\langle a_{lm} a_{l'm'}^* \rangle_{\text{aniso}} = (-i)^{l-l'+1} (4\pi)^2 \frac{9T_0^2}{100} G_{ll'} \xi_{lm;l'm'}^0, \tag{49}$$

$\xi_{lm;l'm'}^0$  is defined in Eq. (10) and

$$G_{ll'} = \int_0^{\infty} k^2 dk P(k) j_l(k\eta_0) j_{l'}(k\eta_0) g(k). \tag{50}$$

Using Eq. (44), we obtain

$$G_{ll'} = \frac{g_0 A_\phi}{4\pi} \int_0^{\infty} \frac{ds}{s^{1+\alpha}} j_l(s) j_{l'}(s). \tag{51}$$

Hence the anisotropic power spectrum, Eq. (14), leads to a correlation between  $l$  and  $l \pm 1$ . This allows us to obtain the theoretical prediction of the statistic,  $S_H(L)$ , which can be compared to  $S_H^{\text{data}}$  in order to determine the best fit value of the power spectrum parameters,  $g_0$  and  $\alpha$ .

## 4 Data analysis

In this section we explain our procedure for extracting the parameters,  $g_0$  and  $\alpha$ , of the anisotropic model. Here we first determine the value of the statistic,  $S_H(L)$ , from data over a chosen multipole range. As mentioned earlier this is denoted  $S_H^{\text{data}}(L)$ . The procedure used for this calculation is the same as that followed in [14, 57]. The main steps in this calculation are given below. We next compute this statistic using the theoretical anisotropic model. The model parameters can then be determined by making a fit to the data value.

We use WMAP’s nine year ILC map [81], denoted WILC9, as well as the SMICA map, provided by the PLANCK team [82]. We use the mask  $KQ85$  and the CMB-union mask, respectively, for these two maps in order to eliminate the foreground contaminated regions. We fill the masked portions by simulated random isotropic CMBR data. The SMICA map as well as the corresponding mask is available at a high resolution with  $N_{\text{side}} = 2048$ . Hence we first generate a full sky CMB data map at this high resolution in this case. Next we smooth the mask boundaries by applying appropriate Gaussian beam [14]. The resulting map is downgraded to a lower resolution with  $N_{\text{side}} = 32$ . This procedure eliminates any breaks at the mask boundaries that might be generated due to our random filling procedure. The WILC9 map is provided only at lower resolution with  $N_{\text{side}} = 512$ . Hence, in this case we generate the full sky map only at this resolution which is subsequently downgraded to a low resolution with  $N_{\text{side}} = 32$ . In this case, the contribution due to detector noise is also included in the simulated data. The detector noise is not included for PLANCK data, since the corresponding noise files are too bulky. In any case, for the multipole range under consideration the contribution due to detector noise is found to be negligible for the WMAP data. Hence it might be reasonable to neglect the detector noise even for PLANCK data in our analysis. The PLANCK team has also provided the SMICA in-painted map. In this case the in-painting procedure [83, 84] has been used in order to reconstruct the masked regions. We use this full sky map also for our analysis.

For each of the three maps, WILC9, SMICA, and SMICA in-painted we first maximize the statistic,  $S_H(L)$ , by making a search over the preferred direction parameters over the chosen multipole. The resulting direction parameters correspond to the choice of our  $z$ -axis. For WILC9 and SMICA maps the masked regions are filled by randomly generated data. Hence for these maps, the results depend on the realization used for the full sky ‘data’ map. The statistic and the corresponding direction parameters,  $(l, b)$ , are computed by taking their average over 100 such filled data maps for both SMICA and ILC.

We first perform the calculation over the entire range of multipoles,  $2 \leq l \leq 64$ , and next repeat it for the multipole

bins,  $l = 2-22, 23-43, 44-64$ . In the latter case, the best fit direction parameters are found to depend on the bin [57]. However, the dependence is relatively mild and we set the direction parameters to be equal to their mean values over the entire range of multipoles,  $l = 2-64$  [57].

Our procedure of filling of masked regions with simulated data is likely to generate some bias, which we estimate through simulations [57]. We correct this bias in the final results. Our bias correction procedure is described below in Sect. 4.1. Our simulations show that the bias generated is relatively small.

The anisotropic power spectrum parameters,  $g_0$  and  $\alpha$ , defined in Eq. (44), are determined by making a fit to the data statistic. The theoretical prediction for the statistic,  $S_H(L)$ , can be obtained by using Eq. (49) for the correlation among different multipoles. We first set  $\alpha = 0$  and extract  $g_0$  for which the theoretical prediction of  $S_H(L)$  agrees with the data value over the entire range of multipoles,  $l = 2 - 64$ . We next use the  $\chi^2$  minimization procedure in order to extract both parameters,  $g_0$  and  $\alpha$ . In this case we use the data in the three multipole bins,  $l = 2-22, 23-43, 44-64$ .

#### 4.1 Bias correction

The bias generated by our procedure of filling masked regions with simulated data in the case of the ILC and the SMICA maps is estimated through simulations by using the method described in [57]. The use of simulations for bias correction is analogous to the procedure used by the WMAP science team [85] in order to correct for the residual foreground contamination in the ILC map. Here we briefly review our bias correction procedure. We first create a full sky CMBR map through simulations which has the same characteristics, including dipole modulation, as the real data. This is obtained by first simulating a full sky isotropic CMBR map. This map is multiplied by the dipole modulation term,  $(1 + A\hat{\lambda} \cdot \hat{n})$ . The direction,  $\hat{\lambda}$ , is taken to be same as that obtained by WMAP [5] and the amplitude,  $A$ , is a free parameter. Subsequently we apply the same mask to this map as used for the real data. The masked regions are finally filled with simulated isotropic CMBR data. This procedure simulates a full sky realization of a map with properties the same as the full sky real map we utilize for our analysis.

We next make a search over the amplitude parameter  $A$  such that the simulated map leads to a statistic,  $S_H$ , which is equal to  $S_H^{\text{data}}$ , the statistic obtained for real data. For each  $A$  the calculation is performed by generating 1000 different realizations of the simulated samples. The output statistic is equal to the average value obtained over these 1000 samples. The error in  $S_H$  is given by the variance over these samples. The final  $A$ , which yields the statistic closest to that obtained by the real data, provides the estimate of this parameter, as well as its error, in real data. We next use this value

of  $A$  in order to obtain the full sky estimate of the statistic. This calculation is performed by generating 1000 full sky realizations of simulated CMBR maps, which have a dipole modulation whose amplitude is the same as the value of  $A$  extracted above. The bias corrected estimate of the statistic,  $S_H$ , is obtained by taking an average of its value over these 1000 maps.

### 5 Results

For the entire multipole range,  $2 \leq l \leq 64$ , the best fit values of  $g_0$  are given in Table 1 for all the three maps. Here we have assumed that the spectral index  $\alpha = 0$ . Hence the function,  $g(k)$ , is equal to a constant,  $g_0$ . The bias corrected statistic as well as the best fit direction parameters, obtained in [57], are also given in Table 1. We find that the bias correction is relatively small, less than 10 % both for WILC9 and SMICA [57]. The extracted values of the dipole modulation amplitude parameter,  $A$ , are given in Ref. [57]. We find that both the direction and the amplitude parameters of the dipole modulation are consistent with those obtained earlier by hemispherical analysis of WMAP [1-4,6,8] and PLANCK [7] data.

We next extract the function,  $g(k)$ , using data in the three multipole bins,  $l = 2-22, 23-43$  and  $l = 44-64$ . We parameterize it in terms of  $g_0$  and the spectral index  $\alpha$ . As explained in Sect. 4, here we set the direction parameters for all the three bins to be equal to the mean parameters over the entire range  $l = 2-64$  [57]. Setting  $\alpha = 0$ , the best fit value of  $g_0$  is found to be  $g_0 = 0.24 \pm 0.06$  with  $\chi^2 = 0.41$  for WILC9 and  $g_0 = 0.23 \pm 0.06$  with  $\chi^2 = 0.15$  for SMICA. For SMICA (in-painted) we obtain  $g_0 = 0.27 \pm 0.07$  with  $\chi^2 = 1.4$  for  $\alpha = 0$ . Hence we find that a zero spectral index for the anisotropic part of the power spectrum provides a good fit to the data. The resulting fit is shown in Fig. 1 as the dotted line. The value of  $\chi^2$  is found to be rather small, especially for the case of SMICA. However, such a small value is not unreasonable in the present case when we fit only three data points. Furthermore the data value in the first bin is found to have a rather large error. Allowing a non-zero value of  $\alpha$  we find that the  $1\sigma$  limit on this parameter is,  $-0.28 < \alpha < 0.28$  and  $-0.46 < \alpha < 0.30$  for WILC9 and SMICA, respectively.

**Table 1** The extracted value of the amplitude  $g_0$  obtained by making a fit in the multipole range  $l = 2 - 64$ . Here we have set  $\alpha = 0$ . The values of the statistic,  $S_H^{\text{data}}$ , and the direction parameters are also given

	$S_H^{\text{data}}(L)$ (mK <sup>2</sup> )	$(l, b)$	$g_0$
WILC9	$0.025 \pm 0.008$	$(227^\circ, -14^\circ)$	$0.28 \pm 0.09$
SMICA	$0.023 \pm 0.006$	$(229^\circ, -16^\circ)$	$0.25 \pm 0.07$
SMICA (in-painted)	$0.027 \pm 0.007$	$(232^\circ, -12^\circ)$	$0.30 \pm 0.08$

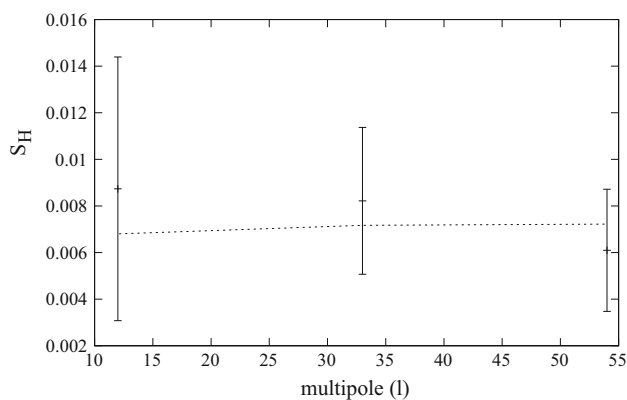


**Fig. 1** The statistic,  $S_H^{\text{data}}$ , as a function of the multipole  $l$  for WILC9. Here the statistic in the three bins is extracted by fixing the direction parameters to be equal to the mean direction over the entire multipole range [57], as given in Table 1. The dotted line is the theoretical fit corresponding to  $\alpha = 0$ ,  $g_0 = 0.24 \pm 0.06$

For SMICA (in-painted), the one sigma limit is found to be  $-0.21 < \alpha < 0.16$ .

Our result that  $\alpha \approx 0$  differs from the result obtained in [76]: a tilt parameter,  $n_*$ , close to zero for the imaginary power spectrum. The two parameters are related as  $\alpha = 1 - n_*$ . Hence in [76], the authors find an anisotropic power which decays with  $k$ . The difference most likely arises since we analyze the signal only in the multipole range,  $2 \leq l \leq 64$ , whereas [76] employs a much larger range  $2 \leq l \leq 400$ . The signal is most likely absent beyond  $l \sim 50$  [76]. We have also explicitly verified that the effective dipole modulation amplitude gets significantly reduced for  $l > 64$ . As we have shown in our paper, the data for low  $l$  is consistent only with  $\alpha \approx 0$ . Hence the results of [76] suggest that a pure power law is not consistent over the larger range of multipoles. In all likelihood, the function  $g(k)$  may be almost independent of  $k$  for low  $k$ , as suggested by our results, and it dies off at larger  $k$ . We postpone a detailed fit which might provide a good description of data over the full range of multipoles to future research.

## 6 Conclusion

We have shown that noncommutative geometry can lead to a dipolar anisotropic power spectrum, which is required to obtain the observed signal of hemispherical anisotropy. This anisotropy can be parameterized in terms of a dipole modulation model, which leads to correlations among the multipoles corresponding to  $l$  and  $l + 1$ . The noncommutative anisotropic power spectrum model also leads to such a correlation. The anisotropic power spectrum,  $g(k) = g_0(k\eta_0)^{-\alpha}$ , is parameterized in terms of the amplitude,  $g_0$ , and the spectral index,  $\alpha$ . The theoretical power spectrum depends on the model of noncommutative geometry. The precise model used

in this paper leads to a power spectrum which, for small  $k$ , grows linearly with  $k$ . The full power spectrum has a complicated dependence on  $\vec{k}$ . In this paper we do not use the precise form of the power spectrum predicted by the theory. Instead we directly extract the parameters,  $\alpha$  and  $g_0$ , from the data. We first set  $\alpha = 0$  and determine the value of  $g_0$  by making a fit over the entire multipole range,  $2 - 64$ . The best fit value is found to be  $g_0 = 0.28 \pm 0.09$  for WILC9. We next determine these parameters by making a fit over the three multipole bins,  $l = 2-22$ ,  $23-43$  and  $l = 44-64$ . In this case again we first set,  $\alpha = 0$ . The best fit leads to  $g_0 = 0.24 \pm 0.06$  for WILC9. This leads to a good fit to the data with  $\chi^2 = 0.41$ . Furthermore we find the one sigma limit on  $\alpha$  to be  $-0.28 < \alpha < 0.28$  for WILC9. There are many indications that the signal of the dipole modulation decays for large  $l$  values. Hence the data suggests that the anisotropic power,  $g(k)$ , is independent of  $k$  for small  $k$ , which gives a dominant contribution in the range  $2 \leq l \leq 64$ , but it decays for larger values of  $k$ .

We conclude that the observed hemispherical anisotropy might represent the first observational signature of noncommutative geometry and hence of quantum gravity.

**Acknowledgments** We acknowledge the use of Planck data available from NASA's LAMBDA site (<http://lambda.gsfc.nasa.gov>). Some of the results in this paper have been derived using the Healpix package [86]. We are extremely grateful to A. P. Balachandran and Rajesh Gopakumar for very useful discussions on noncommutative spacetimes. We also thank James Zibin and Anupam Kumar for useful discussions.

**Open Access** This article is distributed under the terms of the Creative Commons Attribution License which permits any use, distribution, and reproduction in any medium, provided the original author(s) and the source are credited.

Funded by SCOAP<sup>3</sup> / License Version CC BY 4.0.

## References

1. H.K. Eriksen et al., *ApJ* **605**, 14 (2004)
2. H.K. Eriksen et al., *ApJL* **660**, L81 (2007)
3. A.L. Erickcek, M. Kamionkowski, S.M. Carroll, *Phys. Rev. D* **78**, 123520 (2008)
4. F.K. Hansen et al., *ApJ* **704**, 1448 (2009)
5. J. Hoftuft et al., *ApJ* **699**, 985 (2009)
6. F. Paci et al., *MNRAS* **434**, 3071 (2013)
7. P. Ade, et al., Planck 2013 Results—XXIII. [arXiv:1303.5083](https://arxiv.org/abs/1303.5083)
8. F. Schmidt, L. Hui, *Phys. Rev. Lett.* **110**, 011301 (2013)
9. Y. Akrami et al., *ApJL* **784**, L42 (2014)
10. C. Gordon et al., *Phys. Rev. D* **72**, 103002 (2005)
11. C. Gordon, *ApJ* **656**, 636 (2007)
12. S. Prunet et al., *Phys. Rev. D* **71**, 083508 (2005)
13. C. Bennett et al., *ApJS* **192**, 17 (2011)
14. P.K. Rath, P. Jain, *JCAP* **12**, 014 (2013)
15. E.P. Donoghue, J.F. Donoghue, *Phys. Rev. D* **71**, 043002 (2005)
16. D. Hanson, A. Lewis, *Phys. Rev. D* **80**, 063004 (2009)
17. C.M. Hirata, *JCAP* **09**, 011 (2009)
18. R. Fernandez-Cobos et al., [arXiv:1312.0275](https://arxiv.org/abs/1312.0275) (2013)

19. A.L. Erickcek, C.M. Hirata, M. Kamionkowski, Phys. Rev. D **80**, 083507 (2009)
20. A. Berera, R.V. Buniy, T.W. Kephart, JCAP **10**, 016 (2004)
21. L. Ackerman, S.M. Carroll, M.B. Wise, Phys. Rev. D **75**, 083502 (2007)
22. C.G. Boehmer, D.F. Mota, Phys. Lett. B **663**, 168 (2008)
23. T.R. Jaffe et al., ApJ **644**, 701 (2006)
24. T. Koivisto, D.F. Mota, Phys. Rev. D **73**, 083502 (2006)
25. K. Land, J. Magueijo, MNRAS **367**, 1714 (2006)
26. M. Bridges et al., MNRAS **377**, 1473 (2007)
27. L. Campanelli, P. Cea, L. Tedesco, Phys. Rev. D **76**, 063007 (2007)
28. T. Ghosh, A. Hajian, T. Souradeep, Phys. Rev. D **75**, 083007 (2007)
29. A. Pontzen, A. Challinor, MNRAS **380**, 1387 (2007)
30. T. Koivisto, D.F. Mota, JCAP **08**, 021 (2008)
31. T. Kahnashvili, G. Lavrelashvili, B. Ratra, Phys. Rev. D **78**, 063012 (2008)
32. S.M. Carroll, C.-Y. Tseng, M.B. Wise, Phys. Rev. D **81**, 083501 (2010)
33. M. Watanabe, S. Kanno, J. Soda, Prog. Theor. Phys. **123**, 1041 (2010)
34. P. Aluri, S. Panda, M. Sharma, S. Thakur, JCAP **1312**, 003 (2013)
35. Z. Chang, S. Wang, Eur. Phys. J. C **73**, 2516 (2013)
36. L. Wang, A. Mazumdar, Phys. Rev. D **88**, 023512 (2013)
37. A. Mazumdar, L. Wang, JCAP **10**, 049 (2013)
38. Y.-F. Cai, W. Zhao, Y. Zhang, Phys. Rev. D **89**, 023005 (2014)
39. Z.-G. Liu, Z.-K. Guo, Y.-S. Piao, Phys. Rev. D **88**, 063539 (2013)
40. Z.-G. Liu, Z.-K. Guo, Y.-S. Piao, arXiv:1311.1599 (2014)
41. Z. Chang, X. Li, S. Wang, arXiv:1307.4542 (2013)
42. Z. Chang, S. Wang, arXiv:1312.6575 (2013)
43. S. Ghosh, S. Phys. Rev. D **89**, 063518 (2014)
44. S. Panda, M. Sharma, arXiv:1406.3992
45. D. Hutsemekers, A & A **332**, 410 (1998)
46. P. Jain, J.P. Ralston, Mod. Phys. Lett. A **14**, 417 (1999)
47. A. de Oliveira-Costa et al., Phys. Rev. D **69**, 063516 (2004)
48. J.P. Ralston, P. Jain, Int. J. Mod. Phys. D **13**, 1857 (2004)
49. D.J. Schwarz et al., Phys. Rev. Lett. **93**, 221301 (2004)
50. A.K. Singal, ApJL **42**, L23 (2011)
51. P. Tiwari, P. Jain, arXiv:1308.3970 (2013)
52. P.K. Aluri, P. Jain, Mod. Phys. Lett. A **27**, 1250014 (2012)
53. P.K. Rath et al., JCAP **04**, 007 (2013)
54. X. Gao, Phys. Lett. B **702**, 12 (2011)
55. J. McDonald, arXiv:1403.2076 (2014)
56. G. Aslanyan, L.C. Price, K.N. Abazajian, R. Easther, arXiv:1403.5849 [astro-ph.CO]
57. P. Rath, P.K. Aluri, P. Jain, arXiv:1403.2567
58. S. Doplicher, K. Fredenhagen, J.E. Roberts, Spacetime quantization induced by classical gravity. Phys. Lett. B **331**, 33–44 (1994)
59. A. Connes, *Noncommutative Geometry* (Academic Press, London, 1994)
60. J. Madore, *An Introduction to Noncommutative Geometry and Its Physical Applications* (Cambridge University Press, Cambridge, 1999)
61. G. Landi, *An Introduction to Noncommutative Spaces and Their Geometries* (Springer, New York, 1997)
62. J.M. Gracia-Bondía, J.C. Várilly, H. Figueora, *Elements of Noncommutative Geometry* (Birkhäuser, Basel, 2001)
63. E. Akofor, A.P. Balachandran, S.G. Jo, A. Joseph, B.A. Qureshi, JHEP **0805**, 092 (2008)
64. C.S. Chu, B.R. Greene, G. Shiu, Mod. Phys. Lett. A **16**, 2231–2240 (2001). arXiv:hep-th/0011241
65. F. Lizzi, G. Mangano, G. Miele, M. Peloso, JHEP **0206**, 049 (2002). arXiv:hep-th/0203099
66. R. Brandenberger, P.M. Ho, Phys. Rev. D **66**, 023517 (2002). arXiv:hep-th/0203119
67. Q.G. Huang, M. Li, JHEP **0306**, 014 (2003). arXiv:hep-th/0304203
68. Q.G. Huang, M. Li, JCAP **0311**, 001 (2003). arXiv:astro-ph/0308458
69. S. Tsujikawa, R. Maartens, R. Brandenberger, Phys. Lett. B **574**, 141–148 (2003). arXiv:astro-ph/0308169
70. A.P. Balachandran, A.R. Queiroz, A.M. Marques, P. Teotonio-Sobrinho, arXiv:0706.0021 [hep-th]
71. L. Barosi, F.A. Brito, A.R. Queiroz, JCAP **0804**, 005 (2008). arXiv:0801.0810 [hep-th]
72. A.H. Fatollahi, M. Hajirahimi, Europhys. Lett. **75**, 542–547 (2006). arXiv:astro-ph/0607257
73. A.H. Fatollahi, M. Hajirahimi, Phys. Lett. B **641**, 381–385 (2006). arXiv:hep-th/0611225
74. E. Akofor, A.P. Balachandran, A. Joseph, L. Pekowsky, B.A. Qureshi, Phys. Rev. D **79**, 063004 (2009)
75. T.S. Koivisto, D.F. Mota, JHEP **1102**, 061 (2011). arXiv:1011.2126
76. N.E. Groeneboom, M. Axelsson, D.F. Mota, T.S. Koivisto, arXiv:1011.5353
77. M. Shiraishi, D.F. Mota, A. Ricciardone, F. Arroja, arXiv:1401.7936
78. A. Nautiyal, Phys. Lett. B **728**, 472 (2014)
79. Yi-Fu Cai, Yi Wang, Phys. Lett. B **735**, 108 (2014)
80. D.S. Gorbunov, V.A. Rubakov, *Introduction to the Theory of the Early Universe: Cosmological Perturbations and Inflationary Theory* (World Scientific, Singapore, 2011)
81. C.L. Bennett et al., APJS **208**, 20 (2013)
82. P. Ade et al., Planck 2013 Results—I. arXiv:1303.5062
83. P. Abrial et al., Stat. Methodol. **5**, 289 (2008)
84. K.T. Inoue, P. Cabella, E. Komatsu, Phys. Rev. D **77**, 123539 (2008)
85. G. Hinshaw et al., ApJS **170**, 288 (2007)
86. K. Gorski et al., ApJ **622**, 759 (2005)